UC Berkeley
UC Berkeley Previously Published Works

Title

In vivo fluorescence imaging of biomaterial-associated inflammation and infection in a minimally invasive manner

Permalink

https://escholarship.org/uc/item/2df0p6hg

Journal

Journal of Biomedical Materials Research Part A, 103(1)

ISSN

1549-3296

Authors

Suri, Shalu
Lehman, Susan M
Selvam, Shivaram
et al.

Publication Date

2015

DOI

10.1002/jbm.a.35162

Peer reviewed

In Vivo Fluorescence Imaging of Biomaterial-Associated Inflammation and Infection in a Minimally-Invasive Manner

Shalu Suri[a,b], **Susan M. Lehman**[a,b], **Shivaram Selvam**[a,b], **Khalilah Reddie**[b], **Santanu Maity**[c], **Niren Murthy**[c], and **Andrés J. García**[a,b]

[a]Woodruff School of Mechanical Engineering, Georgia Institute of Technology, Atlanta, Georgia, USA

[b]Petit Institute for Bioengineering and Bioscience, Georgia Institute of Technology, Atlanta, Georgia, USA

[c]Department of Bioengineering, University of California Berkeley, Berkeley, California, USA

Abstract

Implant-associated inflammation and bacterial infection severely limit the functional performance of medical devices and are a major cause of implant failure. Therefore, it is crucial to develop methodologies to monitor/image implant-associated aseptic inflammation and bacterial infection in a minimally invasive manner. Here, we exploited near-infrared fluorescence (NIRF) molecular probes injected locally at the implant site to perform minimally invasive, simultaneous imaging of inflammation and infection associated with implanted polymer disks. The hydro-sulpho-Cy5 (H-s-Cy5) probe detected reactive oxygen species associated with inflammatory responses to both aseptic and biofilm-containing implants, whereas diaminocyanine sulphonate (DAC-S) selectively detected nitric oxide (NO) associated with a biofilm on the biomaterial at acute time points (<4 days). This imaging modality also allows longitudinal monitoring because of high specificity and fast clearance rate of the fluorescent probes. Taken together, these NIRF molecular probes represent a useful tool to directly image inflammatory responses and infections associated with implanted devices for the diagnosis of device-associated inflammation and infection as well as the development of effective therapies.

Keywords

implant; bacteria; macrophage; ROS; nitric oxide; fibrosis; near-infrared fluorescence

Introduction

Implantation of medical devices results in a dynamic inflammatory response comprising biomolecule adsorption, neutrophil and macrophage recruitment to the implant site, adhesion, and activation (e.g., cytokine release), macrophage maturation/fusion, fibrous

Corresponding author: Andrés J. García, Ph.D. Woodruff School of Mechanical Engineering Petit Institute for Bioengineering and Bioscience 315 Ferst Drive, 2310 Petit Biotechnology Bldg. Atlanta, GA 30332-0363, U.S.A. Phone: 1-404-894-9384, andres.garcia@me.gatech.edu.

encapsulation and wound healing/tissue remodeling (1, 2). Device-associated inflammation limits tissue integration and biological performance of devices in patients. In addition, in many cases, implantation is followed by infections, such as catheter-associated bloodstream and surgical site infections, resulting in substantial morbidity and mortality (3). Of note, 50% of hospital-acquired infections involve device-associated infections, contributing significantly to the high cost of caring for patients (4). Conventional analyses of inflammation and infection primarily rely on endpoint analysis such as histology, immunohistochemistry, and biochemical assays that are destructive, invasive and time consuming, and are unable to (1) monitor the inflammatory response, (2) detect biomaterial-associated infections, and (3) determine the course and effectiveness of therapeutics to treat implant-associated inflammation and infection in a minimally invasive fashion. Hence, new methodologies to detect and monitor implant-associated aseptic inflammation and bacterial infections are greatly needed.

Neutrophils and macrophages recruited to the surface of implanted devices play central roles in the inflammatory cascade (1). Among the various bioactive factors and mediators secreted by these inflammatory cells in response to the implant, reactive oxygen species (ROS), which comprise free radicals and peroxides, have been widely implicated to play a central role in the inflammatory response to implanted biomaterials (5-7). Implanted biomaterials induce elevated production of ROS at the tissue-implant interface (8). We recently exploited this ROS response to establish a minimally invasive strategy for *in vivo* imaging of biomaterial-associated inflammation using ROS-responsive hydrocyanine probes (9).

During a bacterial infection at an implant site, nitric oxide (NO), a short lived free radical, is naturally produced by macrophages and neutrophils to kill invading bacterial pathogens (10, 11). NO serves as an effector molecule in macrophage-mediated cytotoxicity and plays an important role in host defense against bacterial infections (12, 13). In particular, high levels of NO are secreted by macrophages in response to bacterial lipopolysaccharides (10). We therefore hypothesized that ROS and NO could serve as selective indicators of device-associated aseptic inflammation versus bacterial infection within the vicinity of an implant (Fig. 1). Using our hydrocyanine probes for ROS (9) and the recently described NO-specific near-infrared sensor diaminocyanine sulphonate (DAC-S) (14), we present a minimally invasive strategy for simultaneous, real-time monitoring of i) implant associated-aseptic inflammation by detecting ROS and ii) bacterial infection by detecting NO released in the vicinity of the implant. This imaging modality has clinical translational potential and could be very beneficial for the development of novel therapies to improve the performance of biomedical devices.

Materials and methods

Synthesis of diaminocyanine sulphonate (DAC-S)

Detailed synthesis, analysis and purification of DAC-S have been described (14). Briefly, 4-amino-3-nitrophenol and sodium hydride were dissolved in anhydrous dimethylforamide (DMF) and stirred under argon for 10 min. A solution of IR-783 was dissolved in DMF and the resultant reaction mixture was stirred for 4 h. The solvent was then removed under

reduced pressure and the crude product was purified by silica gel chromatography to afford the desired product as a dark green solid.

The dark green solid was dissolved in methanol (MtOH), concentrated hyaluronic acid and stannous chloride dihydrate were added to the reaction mixture and stirred at room temperature overnight under an argon atmosphere. The reaction mixture was then neutralized with 6 N sodium hydroxide, and the resultant insoluble salt was removed by filtration. The filtrate was concentrated under reduced pressure and the residue was dissolved again in MtOH and the insoluble salt was removed by filtration. The solvent was removed under reduced pressure and the resultant crude product was purified by silica gel chromatography. Further purification was performed by semi-preparative HPLC to again yield a dark green solid. The synthesis of the final compound was verified by H-NMR and mass spectrometry.

Synthesis of sulfo-Cy5 and H-sulfo-Cy5

Extracellular, water-soluble sulfo-Cy5 dye was synthesized using a soluble polymer-supported synthesis strategy as described previously (15). Briefly, poly(ethylene glycol) (PEG)-bound aniline was reacted with 1,1,3,3-tetramethoxypropane in glacial acetic acid to give PEG-bound-4-(3-methoxyallylideneamino)benzonic acid ester (1). Subsequent reaction of (1) with 1-ethyl-2,3,3-trimethylindolenium-5-sulfonate in glacial acetic acid formed immobilized activated PEG-bound tetramethine hemicyanine (2). Reaction of (2) with 1-carboxypentylnyl)-2,3,3-trimethylindolenium-5-sulfonate finally yielded the pentamethine cyanine dye. The reaction mixture was cooled to room temperature and a blue gummy product was precipitated with ethyl acetate and washed with dichloromethane to remove all PEG-bound materials. The synthesized sulfo-Cy5 dye was then further purified by silica gel chromatography. The structure of the final product was confirmed by H-NMR and mass spectrometry.

Hydrocyanine H-sulfo-Cy5 (H-s-Cy5) was prepared by reduction of sulfo-Cy5 with sodium borohydride (16). Briefly, 1 mg of sulfo-Cy5 dye was dissolved in 4 mL MtOH and reduced by adding 2 mg of sodium borohydride. The reaction mixture was then stirred for 5 min and the solvent was removed under reduced pressure. The resulting solid was nitrogen capped and was either used immediately or stored overnight at −20 °C.

In vitro probe testing

In a 96 well plate, both H-s-Cy5 and DAC-S (1 μL from 0.5 mg/mL stock) were separately reacted with 10 μL H_2O_2 (500 μM) and 5.6 μL iron heptahydrate (500 μM). H_2O_2 reacts with iron heptahydrate and forms hydroxyl radical (OH•) (17). Similarly, H-s-Cy5 and DAC-S were also reacted separately with 2 μL of 0.5 mg/mL NOC-7. NOC-7 is a nitric oxide (NO) donor and releases NO in solution under physiological conditions.

Pseudomonas aeruginosa biofilms on PET disks

P. aeruginosa PsAer-9 strain was originally isolated from a urinary catheter biofilm by R. Donlan, Centers for Disease Control and Prevention. It forms reproducible *in vitro* biofilms on different polymer surfaces when grown in low nutrient media. Implants were prepared

using sterile, endotoxin-free polyethylene terephthalate (PET) disks (8 mm diameter). Disks were placed in 3 mL synthetic interstitial fluid (18) and incubated at 37°C for 5 h on an orbital shaker at 165 rpm. For biofilm implants, 50 µL of an overnight *P. aeruginosa* PsAer-9 culture in LB was added to each well prior to the 5 h incubation. Prior to implantation, each disk was dipped in cell-culture grade Dulbecco's phosphate-buffered saline. The mean initial inoculum for biofilm implants was determined by processing extra implants according to the same protocol described for post-explantation processing. Pilot studies were performed to select inoculum conditions to produce a sub-lethal infection.

Biomaterial implantation

PET disks, either sterile and endotoxin-free or bearing a surface-associated biofilm, were implanted subcutaneously following IACUC-approved procedures in 6-8 week old male BALB/c mice (Jackson Laboratories) anesthetized by isofluorane. A single 1-cm incision was made on the dorsum proximal to the spine, and a subcutaneous pocket laterally spanning the dorsum was created. Sterile disks (two per subject on either side of the spine) were implanted, and the incision was closed using sterile stainless steel wound clips (Reflex 7). Mice recovered from anesthesia in less than 5 minutes after which they were given a subcutaneous injection of buprenorphine (0.03 mg/kg). Mice undergoing the same surgical procedure but receiving no biomaterial implants were used as sham controls to account for surgery-associated trauma/inflammation. N 6 mice were used per group for each animal experiment.

Probe clearance analysis

Mice were injected with various concentrations (0.1, 0.05, or 0.02 mg/mL) of DAC-S dissolved in phosphate-buffered saline (PBS). For H-s-Cy5 clearance, mice were injected with 1 mg/mL of H-s-Cy5 dissolved in PBS. 50 µL of either H-s-Cy5 or DAC-S was injected near the vicinity of the implant. Thirty minutes after probe injection, the animal was anesthetized and the whole body of the animal was placed in an IVIS Lumina® Bioimaging System (Xenogen) and scanned in the NO (ex: 780 nm; em: 820 nm) channel for DAC-S or Cy5 (ex: 640 nm; em: 720 nm) channel for H-s-Cy5. Fluorescence was integrated using Living Image® software Version 3.1 (Xenogen). Probe injection was given only on day 1 and bioimaging was performed on day 1, 4 and 7 to assess probe clearance.

In vivo imaging of biomaterial-associated inflammation

Sterile or biofilm-containing PET disks were implanted subcutaneously. DAC-S (0.02 mg/mL) and H-s-Cy5 (1 mg/mL) were dissolved in 1 mL PBS. At 1, 4, and 7 days post-implantation, probe mixture (50 µL) was injected near the vicinity of the implant. Thirty minutes after probe injection, the animal was anesthetized and the whole body of the animal was placed in an IVIS Lumina® bioimaging system (Xenogen) and scanned in the Cy5 (ex: 640 nm; em: 720 nm) and NO (ex: 780 nm; em: 820 nm) channels respectively. Fluorescence was integrated using Living Image® software Version 3.1 (Xenogen). Because values for absolute fluorescence efficiency vary from experiment to experiment due to slight experimental variations in probe preparation, reaction time, and imaging conditions (room/

camera temperature, animal orientation), only groups within the same experiment were compared.

Bacterial counts on explants

Mice were sacrificed 7 days post-implantation and the PET disks were carefully explanted with the surrounding tissue. Each explanted disk was processed as previously described for biofilm removal (19, 20). Briefly, tubes were placed in a water bath sonicator for successive intervals of 10 min, 5 min, and 30 s, each followed by 30 s of vortexing. The resulting suspension was serially diluted and plated on Trypticase Soy Agar overnight at 37°C to determine CFU/implant.

Statistical analyses

Data are reported as average mean ± s.e.m. Statistical analysis was performed by repeated measures ANOVA in GraphPad. Pair-wise comparisons were performed using Tukey post-hoc test with P 0.05 considered significant. Bacterial counts were $\log_{10}$-transformed prior to analysis.

Results

H-s-Cy5 and DAC-S as specific fluorescent probes for OH• and NO

We first performed *in vitro* testing of the NIRF probes to demonstrate the high sensitivity and selectivity of each probe for ROS and NO (Fig. 2). This assay simply tested probe sensitivity and specificity and was not designed to mimic any in vivo conditions. H-s-Cy5 and DAC-S were separately reacted with OH• and NO. H-s-Cy5 emits fluorescence in the presence of OH• but not NO. Conversely, DAC-S emits fluorescence when reacted with NO but not OH•. These results confirm the specificity of H-s-Cy5 and DAC-S for OH• and NO, respectively. Furthermore, the probes only fluoresce in their respective channels and there was minimal bleed-through observed between the channels. Finally, control experiments with biofilms demonstrated no signal generation for each probe in the presence of bacteria or their metabolites.

In vivo probe clearance

We next examined injected probe clearance in the vicinity of implanted biomaterials. This is a crucial experiment in order to use these probes as sensors to monitor inflammation over time in the same animal. We examined probe clearance for various probe concentrations to determine residual fluorescence from the probes injected at previous time points. Figure 3A and B demonstrate that at concentrations of 0.1 mg/mL and 0.05 mg/mL, DAC-S does not clear by day 4 or even day 7 for either sterile or infected implants. Furthermore, we observed higher fluorescence signals on day 4 compared to day 1. We attribute the higher signal at day 4 compared to signal at day 1 for the higher probe concentrations to inadequate probe clearance from the site and continuous NO production. However, at a concentration of 0.02 mg/mL, the fluorescence signal decreased to background levels by day 4 indicating that there was no residual probe left at the injection site. Furthermore, the fluorescence signal intensity at day 1 was comparable to that of higher probe concentrations on day 1 indicating that this concentration was sufficient to obtain a reliable fluorescence signal to detect NO.

We similarly examined the clearance of the H-s-Cy5 probe. As shown in Figure 3C and D, when injected at 1 mg/mL, H-s-Cy5 signal decreased to background levels by day 4 indicating no residual probe remaining at injection site. From the probe clearance experiment, we established the optimal concentration of these fluorescent probes to be used for longitudinal monitoring of inflammation and infection.

In vivo imaging of biofilm-associated and aseptic inflammation

We next evaluated these NIRF probes in a longitudinal monitoring experiment where we delivered sequential doses of H-s-Cy5 and DAC-S to track ROS and NO production in the same animal (Fig. 4). For the DAC-S probe for NO, fluorescence signal increased over time ($p < 0.001$) and was dependent on the whether the implanted biomaterial was sterile or infected ($p < 0.043$). Mice receiving biofilm-containing implants exhibited 35% (day 1) and 22% (day 4) higher DAC-S fluorescence intensity compared to sterile implants. No differences in fluorescence intensity were detected between sterile implants and sham controls. These results show increases in NO production associated with biomaterials with biofilm and demonstrate that the DAC-S probe can selective distinguish implants with biofilm from sterile implants or surgical sites without implant for these acute time points. By day 7, the DAC-S signal increased for all groups and there were no differences in DAC-S signal among groups. We attribute the time-dependent increases in DAC-S signal to changes in tissue NO concentration due to NO-producing cells during the foreign body response as well as biofilm-associated inflammation.

For the H-s-Cy5 sensor for ROS, high fluorescence signal was evident for all implant groups at day 1 post-implantation and the signal decreased over time for all groups ($p < 0.001$). At day 1, mice receiving implants with biofilm exhibited higher H-s-Cy5 fluorescence signal compared to mice receiving sterile implants ($p < 0.01$) and sham controls ($p < 0.001$). Additionally, the fluorescence signal for sterile implants was higher that the signal for sham controls ($p < 0.05$). No significant differences in fluorescence signal were detected among groups for day 4 or 7.

Bacterial Counts at Explant

Because it is well established that mice are resistant to bacterial infections and often clear infections at sub-lethal doses, we quantified bacterial counts on implants at day 7 to determine whether the decreases in ROS signal and loss of discrimination power for the NO probe were associated with clearance of the biofilm. Following sacrifice, PET disks were explanted with surrounding connective tissue from mice receiving biofilm implants, and samples were processed for bacterial counts. Indeed, the majority of implants (62%) had no detectable bacterial counts, and there was no correlation ($p = 0.63$) between bacterial counts and fluorescence intensity for either probe at day 7 (Fig. 5).

Discussion

Device-associated infections, such as catheter-associated bloodstream and surgical site infections, result in substantial morbidity and mortality and contribute significantly to the high cost of caring for patients. The inability to directly image inflammatory responses and

infections associated with implanted devices constitutes a major roadblock to the diagnosis of device-associated inflammation and infection as well as the development of effective therapies. There is therefore a great need for the development of minimally invasive approaches to image inflammation and infection *in vivo*. Recent work has centered on using chemiluminescent *S. aureus* strains (Caliper/Xenogen Xen29, 36, and 40) as model self-imaging pathogens for infection studies (21). Similarly, there is also an analogous eGFP-transfected *P. aeruginosa* strain for imaging that has been explored (22). However, these strains have virulence issues that remain to be addressed in infection model validations. In the present study, we evaluated two NIRF molecular probes specific for NO and ROS to discriminate between biofilm-related and aseptic inflammation associated with implanted biomaterials using minimally invasive *in vivo* imaging. These two NIRF probes were selected because of their different specificities for NO and ROS, solubility and cytocompatibility, and non-overlapping spectral characteristics that allow imaging for both probes in the same animal. We demonstrate that DAC-S, a NIRF probe specific for NO, can discriminate between biofilm-containing and sterile implants at acute time points (4 days). Importantly, there was no difference in fluorescence signal for this NO probe between sterile implants and sham (no implant controls), indicating that DAC-S can be used to selectively monitor biomaterial-associated biofilms at these acute time points. We attribute this selectivity for biomaterials with biofilms to increased NO production by neutrophils and macrophages to fight off the bacterial infection. At 7 days post-implantation, there were no differences in DAC-S signal among the groups, and this is partly due to the fact that the bacterial infection was cleared in this model as well as time-dependent increases in DAC-S signal due to NO-producing cells associated with the inflammation.

In contrast, a NIRF probe for ROS, H-s-Cy5, produced significant differences in fluorescent signal associated with inflammatory responses among biofilm-containing implants, sterile implants, and surgical trauma in the absence of an implant (sham controls). This ROS probe provided measures of overall inflammation. The higher ROS signal for biofilm-containing implants compared to sterile implants is attributed to enhanced inflammation associated with the biofilm. Similarly, the elevated ROS levels for the sterile implant compared to the sham control are attributed to the increased inflammation associated with the implant. This result is consistent with our previous analyses using the H-ICG probe (9).

Several NIRF probes have been developed to image bacterial infections *in vivo* (23-29). The sensing mechanism for these probes relies on internalization and metabolic conversion of molecules inside bacteria or molecules with high affinity for bacterial membrane proteins. These sensing mechanisms pose significant challenges for imaging bacteria because the metabolic activity and biochemical profiles in many bacterial species vary among planktonic and biofilm states. In addition, these reports deal with direct injection of bacteria rather than bacteria in a biofilm associated with a biomaterial. As such, we expect that our strategy using NIRF sensors for inflammation as indirect probes for a device-associated infection will overcome these challenges. Indeed, we were able to selectively image inflammation associated with a biofilm-containing implant using the DAC-S probe. From a practical standpoint, the DAC-S probe may be a more suitable candidate to image biomaterial-associated biofilms since it does not detect inflammation associated with aseptic implants

and therefore the signal is directly related to the inflammatory response to the biofilm. In contrast, the ROS probe would require calibration to discriminate between biofilm-containing and sterile implants, and this calibration may vary significantly due to variability among patient, device, implant location, and biofilm characteristics. A critical aspect of our imaging strategy is that imaging probes must reach the implant site in order to react with local reactive species produced by inflammatory cells. The feasibility of successfully using these probes in complex situations where the blood flow is restricted (such as diabetes) or the immune system is compromised remains to be examined.

We demonstrate minimally invasive, longitudinal imaging of aseptic and biofilm-associated inflammation to implanted biomaterials using NIRF molecular probes. NIRF has considerable translational potential because of excellent optical characteristics in terms of high sensitivity and low autofluorescence, tissue penetration (up to several centimeters in various human tissues), reliable 3-D image reconstruction, high sensitivity, and clinical compatibility with existing fluorescence imaging instrumentation (30). A limitation of the present study was that the biofilm was cleared by the host during the longitudinal imaging window. This result complicated interpretation of imaging data in terms of longitudinal tracking of the biofilm. Longitudinal imaging experiments with more robust infection models, as well as studies evaluating therapeutic strategies, and correlation to histological analyses are necessary to fully establish the potential of these NIRF molecular probes for imaging device-associated inflammation. Finally, the present study was limited to implants below the murine dermis where spectral emission attenuation is minimal; follow-up studies with deeper implant sites and thicker dermal tissue (such as that in higher mammal) are required to ascertain the translational potential of this imaging strategy.

Conclusions

We evaluated two NIRF probes specific for NO and ROS to discriminate between biofilm-related and aseptic inflammation associated with implanted biomaterials using minimally invasive *in vivo* imaging. DAC-S, a NIRF probe specific for NO, discriminated between biofilm-containing and sterile implants at acute time points. Importantly, there was no difference in fluorescence signal for this NO probe between sterile implants and sham (no implant controls), indicating that DAC-S can be used to selectively monitor biomaterial-associated biofilms. In contrast, H-s-Cy5, a NIRF probe for ROS, provided measures for overall inflammation and produced significant differences in fluorescent signal associated with inflammatory responses among biofilm-containing implants, sterile implants, and surgical trauma in the absence of an implant. These NIRF molecular probes represent a useful tool to directly image inflammatory responses and infections associated with implanted devices for the diagnosis of device-associated inflammation and infection as well as the development of effective therapies.

Acknowledgments

References

1. Anderson JM, Rodriguez A, Chang DT. Foreign body reaction to biomaterials. Semin Immunol. 2008; 20(2):86–100. PMCID: 2327202. [PubMed: 18162407]

2. Franz S, Rammelt S, Scharnweber D, Simon JC. Immune responses to implants - a review of the implications for the design of immunomodulatory biomaterials. Biomaterials. 2011; 32(28):6692–709. [PubMed: 21715002]

3. Darouiche RO. Device-associated infections: a macroproblem that starts with microadherence. Clin Infect Dis. 2001; 33(9):1567–72. [PubMed: 11577378]

4. Darouiche RO. Treatment of infections associated with surgical implants. N Engl J Med. 2004; 350(14):1422–9. [PubMed: 15070792]

5. Karlsson M, Tang L. Surface morphology and adsorbed proteins affect phagocyte responses to nano-porous alumina. J Mater Sci Mater Med. 2006; 17(11):1101–11. [PubMed: 17122925]

6. Tsaryk R, Kalbacova M, Hempel U, Scharnweber D, Unger RE, Dieter P, et al. Response of human endothelial cells to oxidative stress on Ti6Al4V alloy. Biomaterials. 2007; 28(5):806–13. [PubMed: 17049373]

7. Serrano MC, Pagani R, Pena J, Portoles MT. Transitory oxidative stress in L929 fibroblasts cultured on poly(epsilon-caprolactone) films. Biomaterials. 2005; 26(29):5827–34. [PubMed: 15949548]

8. Hooper KA, Nickolas TL, Yurkow EJ, Kohn J, Laskin DL. Characterization of the inflammatory response to biomaterials using a rodent air pouch model. J Biomed Mater Res. 2000; 50(3):365–74. [PubMed: 10737878]

9. Selvam S, Kundu K, Templeman KL, Murthy N, Garcia AJ. Minimally invasive, longitudinal monitoring of biomaterial-associated inflammation by fluorescence imaging. Biomaterials. 2011; 32(31):7785–92. PMCID: 3159805. [PubMed: 21813173]

10. Stuehr DJ, Marletta MA. Mammalian nitrate biosynthesis: mouse macrophages produce nitrite and nitrate in response to Escherichia coli lipopolysaccharide. Proc Natl Acad Sci U S A. 1985; 82(22):7738–42. PMCID: 391409. [PubMed: 3906650]

11. Miwa M, Stuehr DJ, Marletta MA, Wishnok JS, Tannenbaum SR. Nitrosation of amines by stimulated macrophages. Carcinogenesis. 1987; 8(7):955–8. [PubMed: 2439225]

12. Hibbs JB Jr. Taintor RR, Vavrin Z. Macrophage cytotoxicity: role for L-arginine deiminase and imino nitrogen oxidation to nitrite. Science. 1987; 235(4787):473–6. [PubMed: 2432665]

13. Hibbs JB Jr. Taintor RR, Vavrin Z, Rachlin EM. Nitric oxide: a cytotoxic activated macrophage effector molecule. Biochem Biophys Res Commun. 1988; 157(1):87–94. [PubMed: 3196352]

14. Sasaki E, Kojima H, Nishimatsu H, Urano Y, Kikuchi K, Hirata Y, et al. Highly sensitive near-infrared fluorescent probes for nitric oxide and their application to isolated organs. J Am Chem Soc. 2005; 127(11):3684–5. [PubMed: 15771488]

15. Jiang L, Dou L, Li B. An efficient approach to the synthesis of water-soluble cyanine dyes using poly(ethylene glycol) as a soluble support. Tetrahedron Lett. 2007; 48:5825–29.

16. Kundu K, Knight SF, Willett N, Lee S, Taylor WR, Murthy N. Hydrocyanines: a class of fluorescent sensors that can image reactive oxygen species in cell culture, tissue, and in vivo. Angew Chem Int Ed Engl. 2009; 48(2):299–303. [PubMed: 19065548]

17. Valko M, Morris H, Cronin MT. Metals, toxicity and oxidative stress. Curr Med Chem. 2005; 12(10):1161–208. [PubMed: 15892631]

18. Lennertz RC, Tsunozaki M, Bautista DM, Stucky CL. Physiological basis of tingling paresthesia evoked by hydroxy-alpha-sanshool. J Neurosci. 2010; 30(12):4353–61. PMCID: 2852189. [PubMed: 20335471]

19. Curtin JJ, Donlan RM. Using bacteriophages to reduce formation of catheter-associated biofilms by Staphylococcus epidermidis. Antimicrob Agents Chemother. 2006; 50(4):1268–75. PMCID: 1426991. [PubMed: 16569839]

20. Fu W, Forster T, Mayer O, Curtin JJ, Lehman SM, Donlan RM. Bacteriophage cocktail for the prevention of biofilm formation by Pseudomonas aeruginosa on catheters in an in vitro model system. Antimicrob Agents Chemother. 2010; 54(1):397–404. PMCID: 2798481. [PubMed: 19822702]

21. Niska JA, Shahbazian JH, Ramos RI, Francis KP, Bernthal NM, Miller LS. Vancomycin-rifampin combination therapy has enhanced efficacy against an experimental Staphylococcus aureus prosthetic joint infection. Antimicrob Agents Chemother. 2013; 57(10):5080–6. PMCID: 3811477. [PubMed: 23917317]

22. Malone CL, Boles BR, Lauderdale KJ, Thoendel M, Kavanaugh JS, Horswill AR. Fluorescent reporters for Staphylococcus aureus. J Microbiol Methods. 2009; 77(3):251–60. PMCID: 2693297. [PubMed: 19264102]

23. Leevy WM, Gammon ST, Jiang H, Johnson JR, Maxwell DJ, Jackson EN, et al. Optical imaging of bacterial infection in living mice using a fluorescent near-infrared molecular probe. J Am Chem Soc. 2006; 128(51):16476–7. PMCID: 2531239. [PubMed: 17177377]

24. Bettegowda C, Foss CA, Cheong I, Wang Y, Diaz L, Agrawal N, et al. Imaging bacterial infections with radiolabeled 1-(2′-deoxy-2′-fluoro-beta-D-arabinofuranosyl)-5-iodouracil. Proc Natl Acad Sci U S A. 2005; 102(4):1145–50. PMCID: 545851. [PubMed: 15653773]

25. White AG, Gray BD, Pak KY, Smith BD. Deep-red fluorescent imaging probe for bacteria. Bioorg Med Chem Lett. 2012; 22(8):2833–6. PMCID: 3321076. [PubMed: 22424976]

26. Kong Y, Yao H, Ren H, Subbian S, Cirillo SL, Sacchettini JC, et al. Imaging tuberculosis with endogenous beta-lactamase reporter enzyme fluorescence in live mice. Proc Natl Acad Sci U S A. 2010; 107(27):12239–44. PMCID: 2901431. [PubMed: 20566877]

27. Leevy WM, Gammon ST, Johnson JR, Lampkins AJ, Jiang H, Marquez M, et al. Noninvasive optical imaging of staphylococcus aureus bacterial infection in living mice using a Bis-dipicolylamine-Zinc(II) affinity group conjugated to a near-infrared fluorophore. Bioconjug Chem. 2008; 19(3):686–92. PMCID: 2852891. [PubMed: 18260609]

28. Piatkevich KD, Subach FV, Verkhusha VV. Far-red light photoactivatable near-infrared fluorescent proteins engineered from a bacterial phytochrome. Nat Commun. 2013; 4:2153. PMCID: 3749836. [PubMed: 23842578]

29. Ning X, Lee S, Wang Z, Kim D, Stubblefield B, Gilbert E, et al. Maltodextrin-based imaging probes detect bacteria in vivo with high sensitivity and specificity. Nat Mater. 2011; 10(8):602–7. [PubMed: 21765397]

30. Hilderbrand SA, Weissleder R. Near-infrared fluorescence: application to in vivo molecular imaging. Curr Opin Chem Biol. 2010; 14(1):71–9. [PubMed: 19879798]
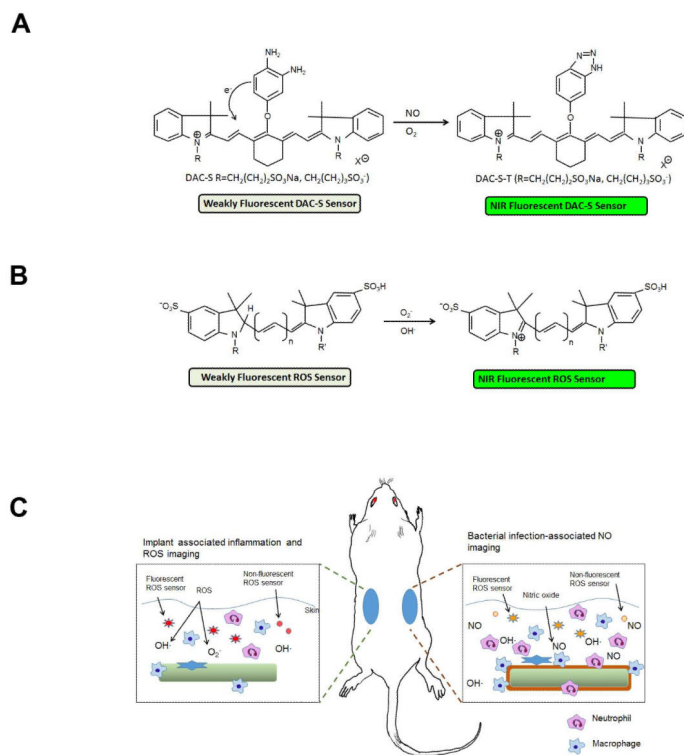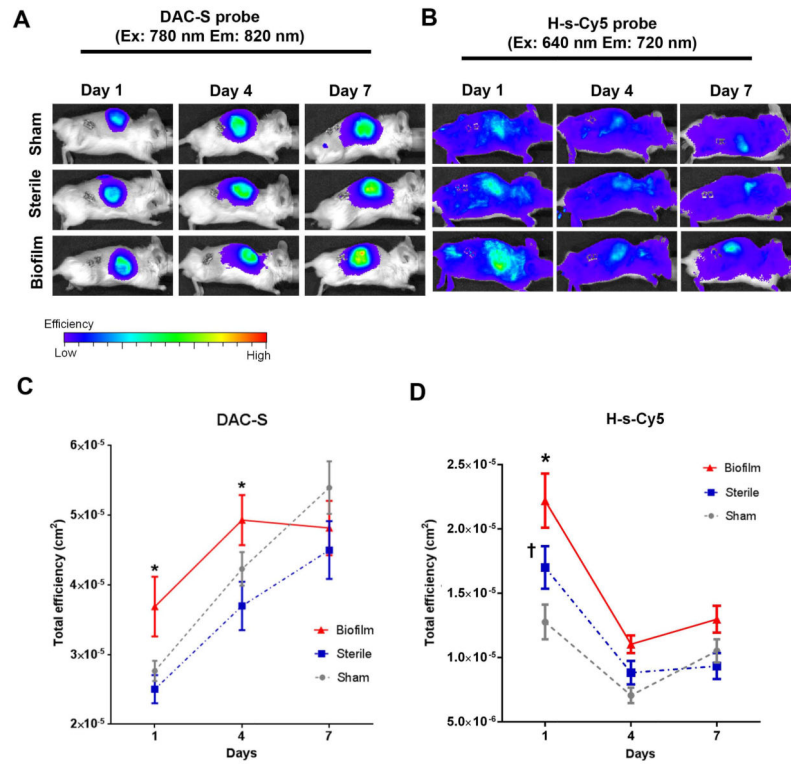
Figure 1.
NIRF imaging of implant-associated inflammation and infection using molecular probes for inflammatory mediators. (A) DAC-S sensor reacts with NO and becomes fluorescent. (B) H-s-Cy5 is oxidized to fluorescent sulpho-Cy5 after reacting with hydroxyl radical and other ROS. (C) Our imaging strategy is based on differential expression profiles for inflammatory mediators between aseptic and biofilm-associated inflammation.
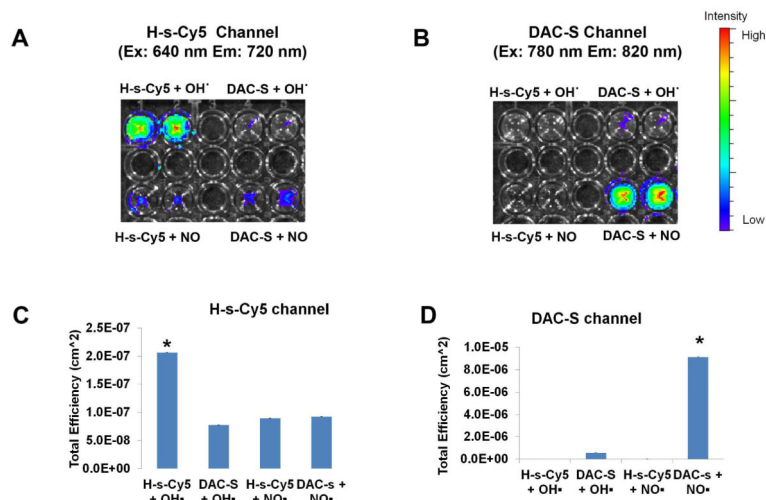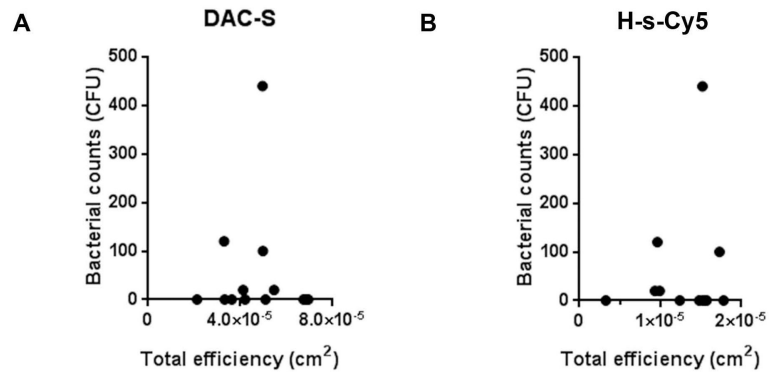
Figure 2.
Specificity of H-s-Cy5 and DAC-S probes for ROS and NO. (A) H-s-Cy5 fluoresces in presence of OH· under the sulpho-Cy5 channel, however background levels of fluorescence were observed in the presence of NO. (B) DAC-S fluoresces in presence of NO in the DAC-S channel, but does not react in the presence of OH·. Furthermore, the probes only fluoresce in their respective channels and there was minimal bleed through observed between the channels. (C) Quantification of fluorescence data for H-s-Cy5 (*p < 0.05). (D) Quantification of fluorescence data for NO (*p < 0.05).
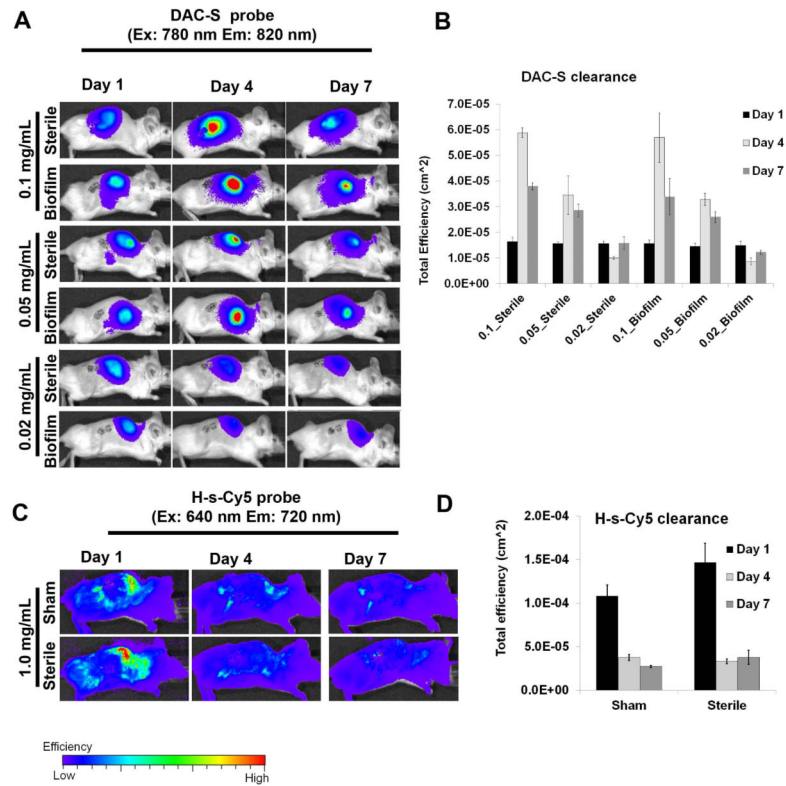
Figure 3.
Clearance study for DAC-S and H-s-Cy5 probes. Mice received subcutaneous implants and were injected with probes on day 1. Imaging was performed on day 1, 4, and 7. (A) Bioimaging scans of mice receiving sterile and biofilm-containing implants for different DAC-S concentrations. (B) Quantification of DAC-S clearance data from fluorescence scans (mean ± s.e.m, n   6 mice per group). (C) Bioimaging scans of mice for sham or sterile implant groups showing H-s-Cy5 clearance (mean ± s.e.m, n   6).

Figure 4.
Longitudinal imaging of implant-associated inflammation and infection after subcutaneous administration of H-s-Cy5 and DAC-S. (A) Bioimaging scans for DAC-S in the sham, implant, and biofilm groups over 7 days. (B) Quantification of DAC-S fluorescence signal (mean ± s.e.m., n 10, * p < 0.05 biofilm vs. sterile). (C) Bioimaging scans for H-s-Cy5 in the sham, implant, and biofilm groups over 7 days. (D) Quantification of H-s-Cy5 fluorescence signal (mean ± s.e.m., n 10, * p < 0.05 biofilm vs. sterile, † p < 0.05 sterile vs. sham).

Figure 5.
Bacterial counts (CFU) from explanted PET disks plotted against their respective NO and H-s-Cy5 fluorescence intensity. No correlation was observed between bacterial counts and fluorescence intensity (p = 0.63).

Table 1

Spectral properties of probes

Probe	Absorbance max (nm)	Emission max (nm)
DAC-S	767	785
H-s-Cy5	649	670